JOURNAL OF GEOPHYSICAL RESEARCH, VOL. ???, XXXX, DOI:10.1029/,

The impact of ozone field horizontal inhomogeneities on nadir-viewing orbital backscatter UV measurements

Martin D. Müller[1,3], Paul Poli[2], Joanna Joiner[1]

M. D. Müller, Leibniz Computing Centre, Barer Straße 21, D-80333 Munich, Germany (martin.d.mueller@web.de)

Paul Poli, Centre National de Recherches Météorologiques, Météo-France, 42 av. Gustave-Coriolis, 31057 Toulouse Cedex 01, France (paul.poli@meteo.fr)

Joanna Joiner, NASA Goddard Space Flight Center Laboratory for Atmospheres, Greenbelt Road, Greenbelt, MD 20771, USA (joanna.joiner@nasa.gov)

[1]NASA Goddard Space Flight Center
Laboratory for Atmospheres, Greenbelt,
USA.

[2]Centre National de Recherches
Météorologiques, Météo-France, Toulouse,
France.

[3]Now at Leibniz Computing Centre,
Munich, Germany.

Abstract. Radiative transfer calculations for nadir-viewing satellites normally assume the atmosphere to be horizontally homogeneous. Yet it has been shown recently that horizontal gradients can lead to significant errors in satellite infrared and microwave soundings. We extend the methodology to backscatter ultra-violet observations of ozone, and present a first estimate of the effect's magnitude. The Solar Backscatter Ultra-Violet/2 (SBUV/2) instrument, a pure nadir sounder, serves as our test bed. Our results indicate that in a vast majority of cases the abovementioned errors can be neglected. However, occurrence of higher errors, particularly at wavelengths longer than 300 nm, coincides with some of the most interesting atmospheric phenomena like tropopause folds and the South polar ozone hole. This leads to a seasonal variation of the magnitude of the effect. Due to the mostly zonal geometry of the ozone distribution, there is also the possibility that biases may be introduced, which is particularly critical if the data are to be assimilated or used to determine trends. The results presented are tested for robustness using different model atmospheres. The influence of horizonal inhomogeneities will be even more pronounced for cross-track sounders and limb viewers, and easier to detect once higher resolution atmopheric models are available. This will be investigated in future studies.

1. Introduction

It has been known for a while that collocations of ground-based measurements with satellite pixels – which rarely sample the same airmass – suffer from errors due to the horizontal variability of the atmospheric quantity considered [e.g. *Lambert et al.*, 1998; *Fioletov et al.*, 1999]. This effect is also relevant for satellite retrievals, and assimilation of retrievals or radiances; Radiative transfer models (RTMs) of the atmosphere commonly assume that the radiances measured by Earth-observing satellites pass through a horizontally homogeneous atmosphere. Depending on the variability of the atmospheric parameters or trace gas species observed, this assumption may induce considerable random and/or systematic errors into the calculations.

For limb-sounders, this realization has led to the development of 2-dimensional retrieval algorithms, which deal with entire atmospheric slices at a time. For instance, [*Worden et al.*, 2004] have found the information content of simulated Thermal Emission Spectrometer CO retrievals to be higher by an order of magnitude for 2-dimensional vs. 1-dimensional retrievals. *Poli and Joiner* [2004] and *Poli* [2004] report that horizontal gradients are also important for Global Positioning System radio occultation soundings. Recently, investigations have begun regarding the effect of temperature inhomogeneities on scanning nadir infrared and microwave sounders [*Joiner and Poli*, 2005]. While generally negligible, the effect was found to be considerable in some situations.

This paper examines the magnitude of ozone inhomogeneities observed by a nadir-viewing instrument merely due to variation of the solar zenith angle (SZA) and solar azimuth angle (SAA). Observation times and locations of the SBUV instrument and an

ozone analysis are used to simulate the effects of horizontal inhomogeneities. To this end, analysis and SBUV data are described in Section 2, along with geometrical considerations. Section 3 focuses on the differences between ozone seen along the slant and nadir ray path. Furthermore, simulated radiance differences for SBUV are computed from three different model fields, and the sensitivity towards the model field is investigated. Section 4 discusses the relevance of the effect in practice, and highlights some considerations for the future.

2. Data and Methods

2.1. Atmospheric model

The global ozone field from an SBUV radiance assimilation system [*Müller et al.*, 2004, 2006] based on earlier work by *Stajner et al.* [2001]; *Riishøjgaard et al.* [2000] is used for representing ozone gradients in the atmosphere. The Chemistry and Transport Model (CTM) used for the assimilation is driven by an online version of the GEOS-4 meteorological assimilation [*Lin*, 2004, and references therein]. This system features a horizontal resolution of 1.25° longitude × 1.0° latitude and generates analyses on 36 pressure levels between 1000 hPa and 0.2 hPa. Since we expect to find significant inhomogeneity effects where strong ozone gradients are present, the periods of 2–4 March 2003 (strong northern hemisphere (NH) ozone gradients) and 16–17 October 2003 (strong south polar ozone gradients) were selected for the various case studies presented.

2.2. SBUV data and geometry

The SBUV/2 instrument used here is a 12-channel pure nadir scanner with a 200 km × 200 km footprint, circling the Earth on an ascending sun-synchronous orbit on board the NOAA-16 satellite, with an Equator crossing at 14:30 local time. We use SBUV as a

shorthand for SBUV/2 throughout this paper. Depending on atmospheric absorption and scattering properties at the wavelength in question (here between 256 nm and 331 nm, see Table 1), not all ozone in a given column will be perceived by the satellite instrument. Figure 1 shows the solar backscatter observation geometry. In order to get an approximate light path for the atmospheric backscattered radiance I, SZA and SAA are calculated for each SBUV observation location and time at the surface. Variation of the SZA with altitude is neglected, and the SAA does not vary with height.

The sun-normalized radiances $\boldsymbol{y}$ measured by the SBUV instrument are usually given in "N-values", whereby

$$\boldsymbol{N} = -100 \log_{10}(\boldsymbol{I}/\boldsymbol{I}_0). \tag{1}$$

With this, the effect of the slanted incidence can be estimated using the linear approximation

$$\Delta \boldsymbol{N} = \boldsymbol{J}(\boldsymbol{x}_{\text{slant}} - \boldsymbol{x}_{\text{nadir}}), \tag{2}$$

where x_{slant} and x_{nadir} are the interpolated analysis fields for slant and nadir path, integrated to yield 21 partial ozone columns on half umkehr layers, as given in the SBUV level 2 retrievals. We can define the Jacobian $\boldsymbol{J}$ of the SBUV RTM for channel i and layer j as

$$(\boldsymbol{J})_{ij} = \frac{\partial N_i}{\partial x_j}. \tag{3}$$

The same approximation is used for the SBUV radiance assimilation [*Müller et al.*, 2004]. For the relatively small profile differences considered, the RTM linearization errors are negligible. A radiance difference of $\Delta N = 1$ translates into a 2.33% relative difference between the corresponding intensities I.

2.3. Approximation of the ray path

To get an estimate for the average photon path through the atmosphere, the effective single scattering altitude for the incoming solar radiation first has to be estimated. Different arguments can be made in this regard, but we chose the peak of the single scattering contribution function (CF) for each SBUV channel as shown in Figure 2. A derivation of these functions can be found in [*Bhartia et al.*, 1996]. The function shapes vary strongly with wavelength, solar zenith angle and ozone profile, less so with the atmospheric temperature profile (all provided with the SBUV level 2 data). Note that for the purpose of calculating the contribution functions, the nadir ozone profile at each pixel location is obtained by linearly interpolating the analysis, i.e. horizontal homogeneity is assumed. The resulting scattering altitudes for all 11 channels considered are depicted in Figure 3. For extreme SZAs, UV radiation merely glances the atmosphere, but the altitude variability is also higher due to the wider range of possible ozone values in the extratropics [e.g. *Hudson et al.*, 2003].

With the direction and penetration depth known, the effective geometric ray path can be calculated using the same method as in [*Poli and Joiner*, 2004]. In this manner, latitude and longitude are obtained for each location where the ray path penetrates one of the 36 analysis levels. The ozone slant profile "seen" by the ray is then calculated by linearly interpolating the model field of each level to these locations. Multiple scattering is not taken into account, nor is the finite range of scattering altitudes for each wavelength. Figure 4 shows the variation of penetration depth and direction for those SBUV pixels which exhibit a noticeable difference between the paths. This gives an impression of the

horizontal separation between the scattering location at nadir, and the point where the ray enters the model atmosphere (about 60 km altitude).

3. Results

In the following, we will compare the differences between the ozone profile seen by the incoming (=slant) and outgoing (=nadir) UV radiation. Obviously, measurements of top-of-atmosphere (TOA) backscattered radiation contain contributions from both path directions For the nadir-viewing SBUV, only the incoming solar ray path is affected by horizontal inhomogeneity, which means that the differences are somewhat averaged over. Calculating exactly the contribution from each direction is beyond the scope of this study.

As can be seen in Figure 4b, interesting pixels for channel 9 cluster around strong gradients in the total ozone field, because this channel penetrates the atmophere already quite well. Figure 4a is somewhat harder to interpret: Comparing with Figure 2 we note that at high SZA the behaviour of channel 8 is similar the channel 9, while at mid to low latitudes it shows more sensitivity, probably because its secondary CF maximum forms around the region of the subtropical tropopause break. But note also that many of the plotted interesting pixels lie in high latitude regions because due to the satellite orbit geometry their ray paths have a strong zonal component. At 70°S latitude where the ozone hole boundary is located, the model resolution is about 110 km $\times$ 50 km (latitude x longitude). Here, gradients along a 200 km longitudinal offset can hence be well resolved. Elsewhere, the ozone gradients have to be much stronger in order to be detectable. Two extreme cases of differences between profiles seen along the nadir and slant paths are depicted in Figure 5. These occurred at the fringe of the southern hemisphere (SH) ozone

hole and at the boundary of an ozone poor region in the NH. The ozone field varies noticeably along the horizontal: Differences of up to 10% are seen in the ozone mixing ratios of slant and nadir paths. This is consistent with the magnitude of slant path related collocation errors reported for zenith-viewing ground instruments as compared to satellites [*Lambert et al.*, 1998].

To assess the critical height regions for these differences globally, their variability was calculated for all 2370 SBUV retrieval locations of 16–17 October 2003 (Figure 7). The sunlight penetration depth depends on both SZA and wavelength, and in turn the differences between observed slant and nadir O_3 profiles depend on penetration depth, SZA and ozone variability above the scattering altitude. Therefore two maxima can be identified in Figure 7: At high SZA, the slant path is longest but the penetration depth is shallow. This leads to a maximum of slant-nadir variability at high altitudes, despite the fact that the ozone distribution is usually quite smooth in the mid-stratosphere and above. A second maximum develops at relatively low SZAs and altitudes for wavelengths reaching the troposphere, mostly in the region around the subtropical tropopause break, where O_3 variability is highest. As already noted by *Joiner and Poli* [2005], the horizontal offsets in the mid- to lower troposphere are too small to cause appreciable ozone differences.

It is also interesting to consider that due to consistent O_3 variation with latitude and systematic patterns in the viewing direction (cf. Figure 4), there are also systematic biases between slant and nadir profiles (Figure 8), even in a global average. Regionally, situations like the ones depicted in Figure 5 may stand for a general trend and thus lead to larger biases. For instance, along the rim of the Antarctic ozone hole, the sun is always seen toward the Equator, and therefore towards higher ozone values, which in turn introduce

a high bias in the nadir vs. slant radiances at altitudes where ozone has been depleted inside the polar vortex.

In order to estimate the robustness of the statistics obtained, the experiment was repeated with the currently operational SBUV v6 profile assimilation system [*Riishøjgaard et al.*, 2000; *Stajner et al.*, 2004] and the underlying CTM without any assimilation (Figure 8b). The differences between the ozone fields are much smaller than the differences between SZA categories or wavelengths. It can hence be concluded that the results described in this paper are also valid for other CTMs and assimilation procedures with similar spatial resolution.

To get an idea of the magnitude of the effect as seen by an orbital UV detector, Figure 6 shows the radiance difference for all SBUV pixels in the March case. For comparison, the measurement noise of the SBUV instruments has been estimated to be generally below 0.5% [*DeLand et al.*, 2004]. The largest differences for this time period occur at the location of the subtropical jetstreams, as the light travels through the tropopause break and its strong ozone gradients. Again, the structures seen are very similar for the three ozone fields introduced for Figure 8b. Interestingly, while the free-running CTM does yield the smallest slant/nadir differences at almost all latitudes, it seems to produce more scatter around the jetstreams. This may be explained by the fact that strong ozone gradients introduced by transport tend to get smoothed out by assimilating the vertically low resolved SBUV observations with imperfect forecast and observation covariance modeling [*Stajner et al.*, 2004; *Müller et al.*, 2006].

The distributions for the radiance differences feature a very strong central peak around zero, with thin tails that spread beyond the measurement noise (Figure 9). This is consis-

tent with what *Joiner and Poli* [2005] found for the AIRS instrument. For the channels between 306 nm and 318 nm as many as 10-20% of the slant-nadir differences are above the SBUV instrument noise level. However, note that in practice this alarming figure is diminished by the fact that the selected ozone hole situation represents a rather extreme case, as can be seen from the seasonal variability of radiance differences shown in Figure 10. Also, while the direct comparison of slant and nadir paths is viable for direct sun ground-based sounders and limb-viewing instruments, the radiance measured by a nadir viewer like SBUV traverses along both slant (incoming) and nadir (backscatter) path. It can be easily shown that with θ denoting the SZA,

$$\boldsymbol{N}_{\text{meas}} \simeq \frac{\boldsymbol{N}_{\text{nadir}} + \boldsymbol{N}_{\text{slant}} \sec\theta}{1 + \sec\theta} \tag{4}$$

is the first-order approximation in $\sec\theta$ for the measured backscattered radiance. Of course, one has to keep in mind that long slant paths, with corresponding appreciable different ozone fields, often occur at high SZA, where $\boldsymbol{N}_{\text{meas}}$ approaches $\boldsymbol{N}_{\text{slant}}$. Furthermore, most modern earth-viewing satellites are cross-track or along-track scanners, where in most cases both incoming and outgoing path are slanted [cf. *Joiner and Poli*, 2005].

4. Conclusions

In general, the errors made through neglecting the horizontal variation of the ozone field fall within the measurement noise of the SBUV instrument. However, while only a relatively small number of observations would benefit from the explicit treatment of their ray path, these tend to lie near the most interesting structures of the ozone field, e.g. ozone (mini-)holes, the subtropical jetstreams and local phenomena like tropopause folds. Especially for field campaigns at high latitudes, which involve comparisons to satellite in-

struments, and for satellite validation in general [e.g. *Fioletov et al.*, 1999; *Lambert et al.*, 1998; *Labow et al.*, 2004] it would be advisable to take slant path offsets into account. Ideally, all ground-based and satellite instruments involved would use the same high-resolution analysis field as a basis for their retrievals. In particular, modern nadir-viewing ozone sounders like the Ozone Monitoring Instrument (OMI) on EOS Aura [*Levelt et al.*, 2006], and the Scanning Imaging Absorption Spectrometer for Atmospheric Chartography (SCIAMACHY) on ENVISAT [*Bovensmann et al.*, 1999] feature wide swaths which introduce a second slant path that may – depending on the geometry – compensate for or exacerbate the inhomogeneity effect.

Future developments in the field are expected to lead to satellite instruments with reduced noise and CTMs with increased accuracy and horizontal resolution. Both factors will render the effects described in this work more important to consider. The same applies to possible future atmospheric chemistry instruments in geostationary orbit or at the Lagrange points. As already mentioned in the introduction, limb-sounding ozone instruments like the one planned for the Ozone Mapping and Profiler Suite (OMPS) [*Dittman et al.*, 2002] are bound to profit most from taking into account horizontal ozone variations.

In [*Joiner and Poli*, 2005] it was reported that accounting for horizontal variability produced smaller differences between forecasted and observed quantities in a meteorological assimilation system for infrared O_3 channels. After having established that the effect described is indeed measurable for backscatter UV instruments as well, our next step will be to modify the radiance assimilation system to take into account horizontal variations. This involves adapting the slant algorithm to the internal assimilation back-

ground field on 55 layers, up to 0.01 hPa, and investigate the impact on the assimilation. The analyzed ozone fields used so far are not ideal for calculating corrections, because the assimilation step has been performed already, and the analysis downsampled to 36 levels. Still, for the limited sample of days investigated, a preliminary calculation (not shown) of simulated radiances for SBUV channels 8 and 9 already shows a small decrease of RMSE vs. the observations on eight months in 2003, if the slant raypath is considered. With this and based on the results obtained thus far, it is hoped that the additional processor cycles needed to calculate a first-order slant path correction turn out to be a worthwhile investment, compared to the computational effort for performing the analysis.

Acknowledgments. The authors wish to thank Ivanka Stajner and Steven Pawson for their extensive help with the GEOS-4 ozone assimilation system. Pawan K. Bhartia provided many valuable insights into the SBUV sensor system. Funding for this research was provided by NASA through a grant from the National Research Council.

References

Bhartia, P. K., R. D. McPeters, C. L. Mateer, L. E. Flynn, and C. Wellemeyer (1996), Algorithm for the estimation of vertical ozone profiles from the backscattered ultraviolet (BUV) technique, *J. Geophys. Res.*, *101*(D13), 18,793–18,806.

Bovensmann, H., J. P. Burrows, M. Buchwitz, J. Frerick, S. Noel, V. Rozanov, K. V. Chance, and A. H. P. Goede (1999), SCIAMACHY - Mission objectives and measurement modes, *J. Atmos. Sci.*, *56*, 125–150.

DeLand, M. T., R. P. Cebula, and E. Hilsenrath (2004), Observations of solar spectral irradiance change during cycle 22 from NOAA-9 Solar Backscattered Ultraviolet Model

2 (SBUV/2), *J. Geophys. Res.*, *109*(D18), 6304.

Dittman, M. G., et al. (2002), Limb broad-band imaging spectrometer for the NPOESS Ozone Mapping and Profiler Suite (OMPS), in *Proc. SPIE - Volume 4814*, edited by W. L. Barnes, pp. 120–130, SPIE.

Fioletov, V. E., J. B. Kerr, E. W. Hare, G. J. Labow, and R. D. McPeters (1999), An assessment of the world ground-based total ozone network performance from the comparison with satellite data, *J. Geophys. Res.*, *104*(D1), 1737–1747.

Hudson, R. D., A. D. Frolov, M. F. Andrade, and M. B. Follette (2003), The Total Ozone Field Separated into Meteorological Regimes. Part I: Defining the Regimes., *J. Atmos. Sci.*, *60*(14), 1669–1677.

Joiner, J., and P. Poli (2005), Note on the effect of horizontal gradients for nadir-viewing microwave and infrared sounders, *Quart. J. Roy. Meteorol. Soc.*, *131*(608), 1783–1792.

Labow, G. J., R. D. McPeters, and P. K. Bhartia (2004), A comparison of TOMS, SBUV & SBUV/2 version 8 total column ozone data with data from groundstations, in *Proc. XX Quadr. Ozone Symposium*, edited by C. Zerefos, Kos, Greece.

Lambert, J.-C., M. V. Roozendael, J. Granville, P. Gérard, P. C. Simon, H. Claude, and J. Staehelin (1998), Comparison of the GOME ozone and NO_2 total amounts at mid-latitude with ground-based zenith-sky measurements, in *Proc. XVIII Quadr. Ozone Symposium*, edited by R. Bojkov and G. Visconti, L'Aquila, Italy.

Levelt, P., G. H. J. van den Oord, M. R. Dobber, A. Malkki, H. Visser, J. de Vries, P. Stammes, J. Lundell, and H. Saari (2006), The Ozone Monitoring Instrument, *IEEE Trans. Geosci. Rem. Sens.*, in press.

Lin, S. J. (2004), A "vertically lagrangian" finite-volume dynamical core for global models, *Mon. Wea. Rev.*, *132*(10), 2293–2307.

Müller, M. D., P. K. Bhartia, and I. Stajner (2004), Assimilation of SBUV version 8 radiances into the GEOS Ozone DAS, in *Proc. XX Quadr. Ozone Symposium*, edited by C. Zerefos, Kos, Greece.

Müller, M. D., I. Stainer, S. Pawson, and P. K. Bhartia (2006), Assimilation of SBUV version 8 radiances into the GEOS-4 Ozone Data Assimilation System, *in preparation.*

Poli, P. (2004), Effects of horizontal gradients on GPS radio occultation observation operators.II: A Fast Atmospheric Refractivity Gradient Operator (FARGO), *Quart. J. Roy. Meteorol. Soc.*, *130*(603), 2807–2825.

Poli, P., and J. Joiner (2004), Effects of horizontal gradients on GPS radio occultation observation operators. I: Ray tracing, *Quart. J. Roy. Meteorol. Soc.*, *130*(603), 2787–2805.

Riishøjgaard, L. P., I. Stajner, and G.-P. Lou (2000), The GEOS ozone data assimilation system, *Adv. Space Res.*, *25*, 1063–1072.

Stajner, I., L. P. Riishøjgaard, and R. B. Rood (2001), The GEOS ozone data assimilation system: Specification of error statistics, *Quart. J. Roy. Meteorol. Soc.*, *127*(573), 1069–1094.

Stajner, I., N. Winslow, R. B. Rood, and S. Pawson (2004), Monitoring of observation errors in the assimilation of satellite ozone data, *J. Geophys. Res.*, *109*(D18), 6309.

Worden, J. R., K. W. Bowman, and D. B. Jones (2004), Two-dimensional characterization of atmospheric profile retrievals from limb sounding observations, *J. Quant. Spectrosc. Radiat. Transfer*, *86*, 45–71.

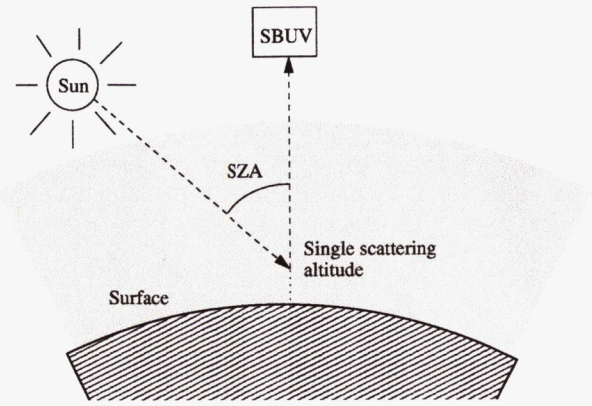

Figure 1. Sketch of the observation geometry.

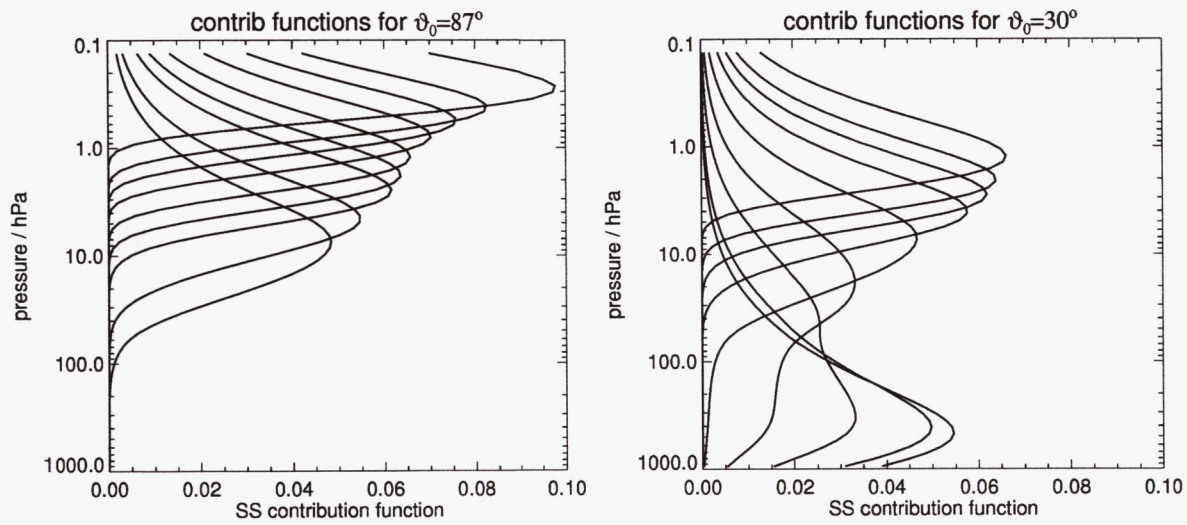

Figure 2. Sample contribution functions for SBUV channels at different SZA for a typical ozone profile (267 DU). Displayed is the single scattering (SS) contribution to the measured radiance, normalized to total radiance: $(\delta I_{SS})/(\delta p)(I_{SS}/I_0)$. The channel wavelengths in nm, from top to bottom are 274, 283, 288, 292, 298, 302, 306, 313 and 318. (Plot adapted from Figure 2 in [*Bhartia et al.*, 1996])

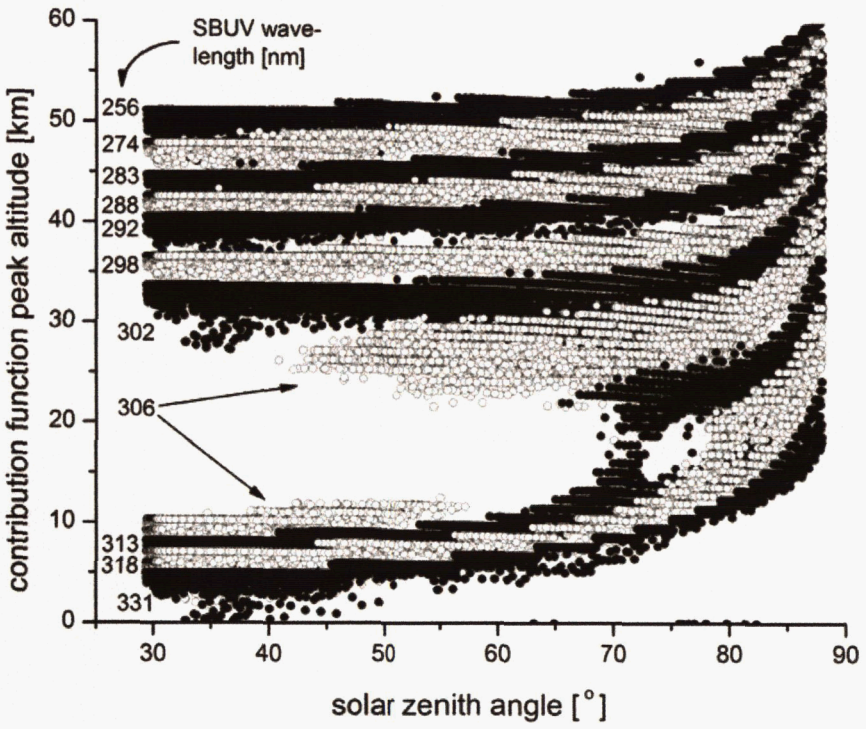

Figure 3. Scattering altitude for all SBUV channels, defined as the maximum of the single scattering CFs. The date range is 3–7 September 2003. The gap around 50 hPa–200 hPa relates to the switch from stratospheric to tropospheric CF maximum. In reality, the transition is more gradual through a nearly bimodal CF shape, as seen in Figure 2b for the 302 nm and 306 nm channels.

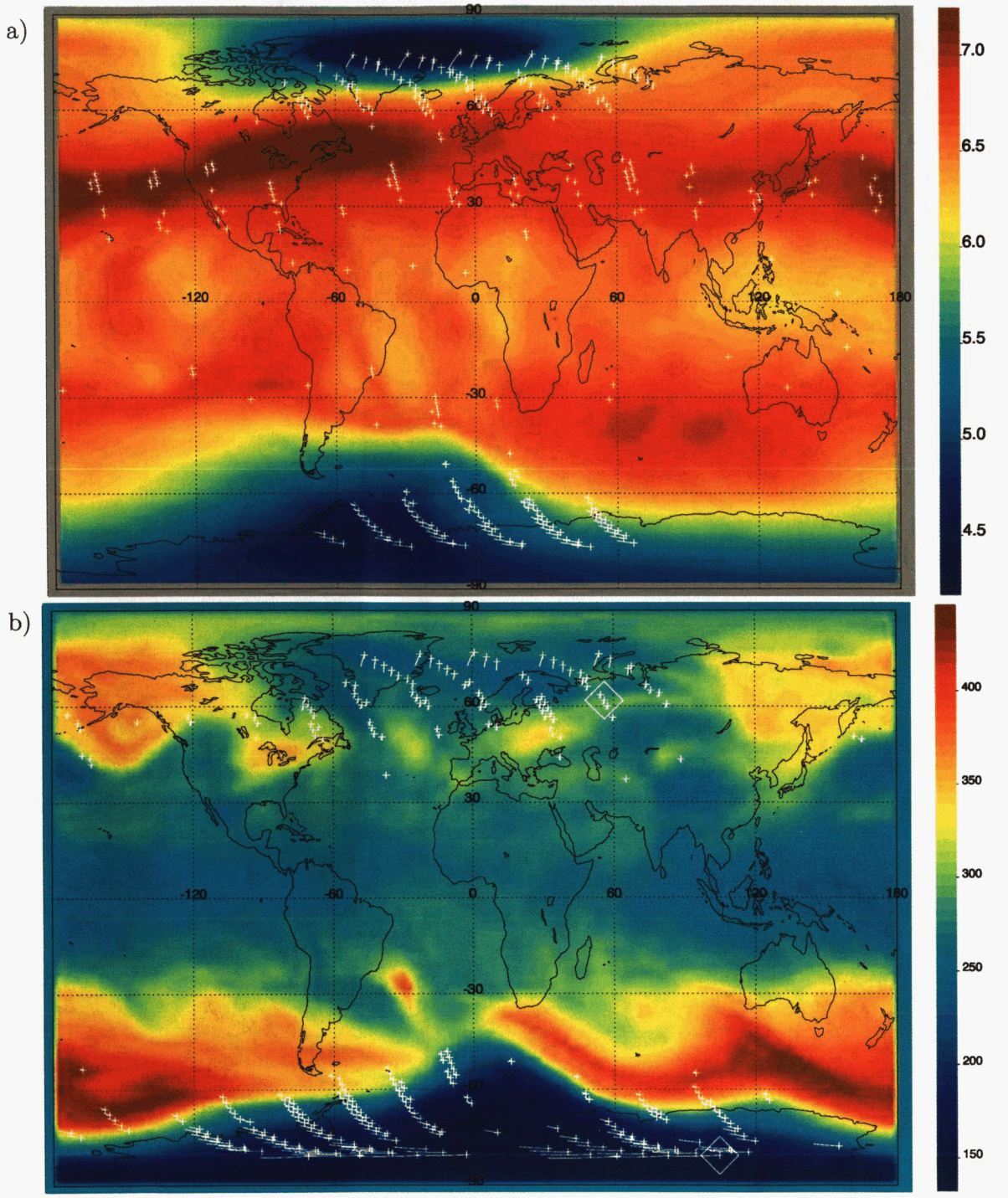

Figure 4. Direction and length of incoming ray path through the model atmosphere, i.e. from 0.2 hPa to scattering altitude. a) SBUV channel 8 (306 nm) superimposed on the ozone volume mixing ratio at 5 hPa (in ppmv) of 17 October 2003, 00:00 UTC, b) same but using channel 9 (313 nm) and the total ozone field, in DU. Crosses denote SBUV nadir points, measured within 24 h around said time. Only the 5% of pixels with the largest radiance differences between simulated slant and nadir paths are shown. The two diamonds are the situations detailed in Figure 5.

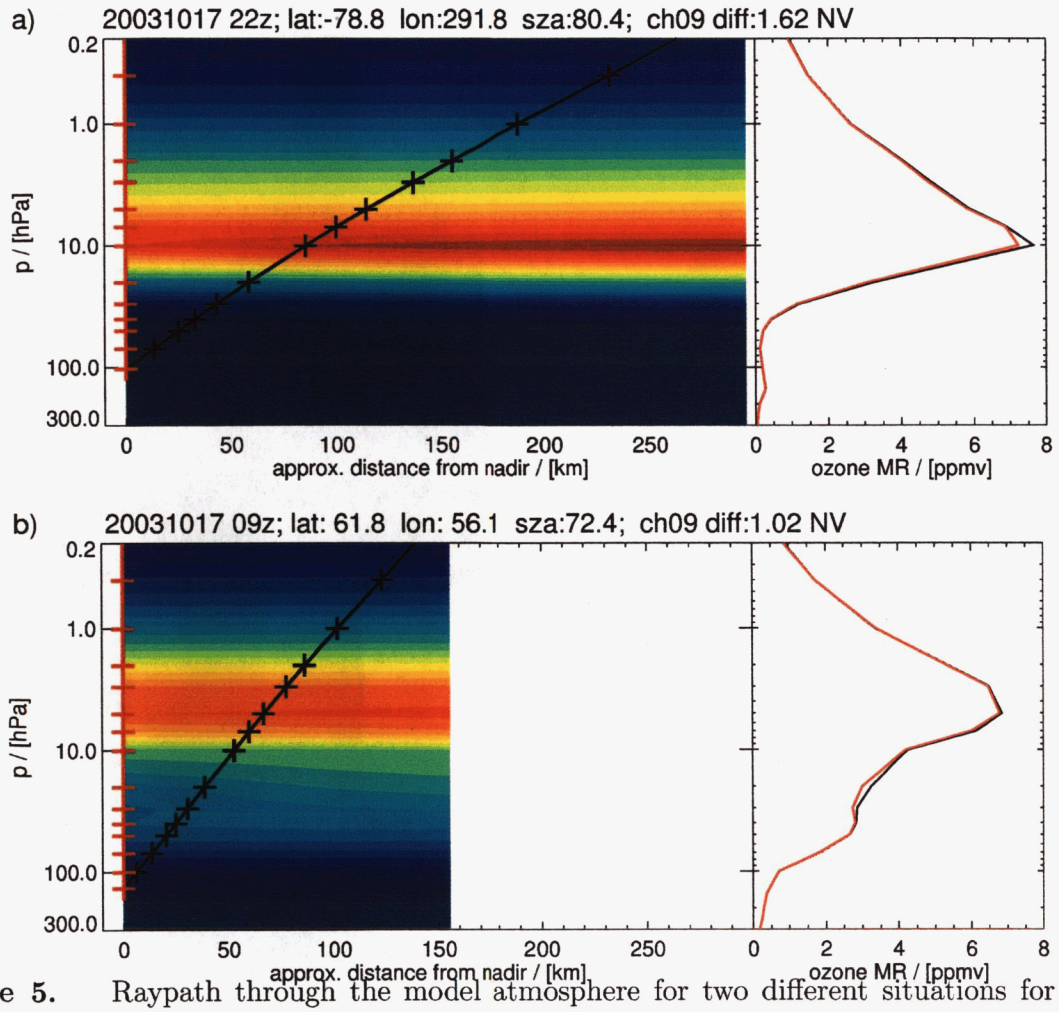

Figure 5. Raypath through the model atmosphere for two different situations for SBUV channel 9 (313 nm).

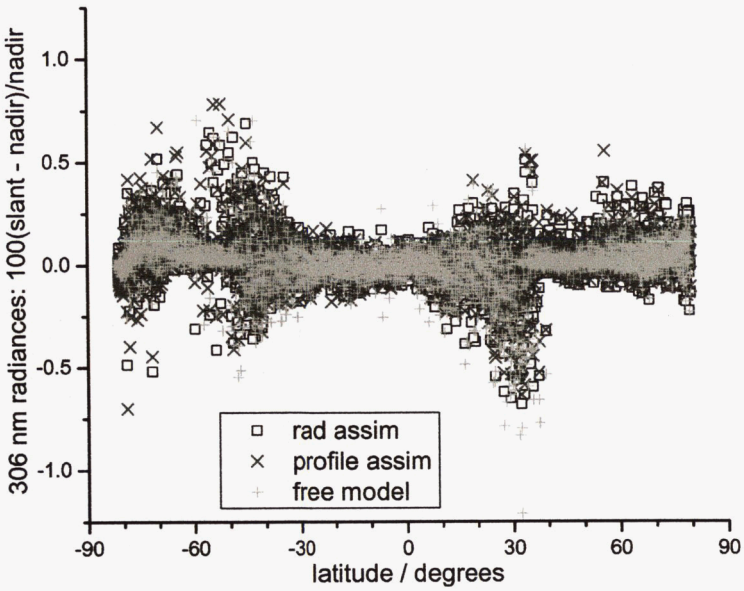

	mean [%]	σ [%]
Radiance assim.	$1.08 \cdot 10^{-2}$	$4.90 \cdot 10^{-2}$
Profile assim.	$8.77 \cdot 10^{-3}$	$4.72 \cdot 10^{-2}$
Free-running model	$3.36 \cdot 10^{-3}$	$5.22 \cdot 10^{-2}$

Figure 6. Differences in radiances calculated for SBUV channel 8 (~306 nm) from slant and nadir profiles of the three different model fields described in the main text, for 2–4 March 2003. The table lists the respective mean difference and standard deviation.

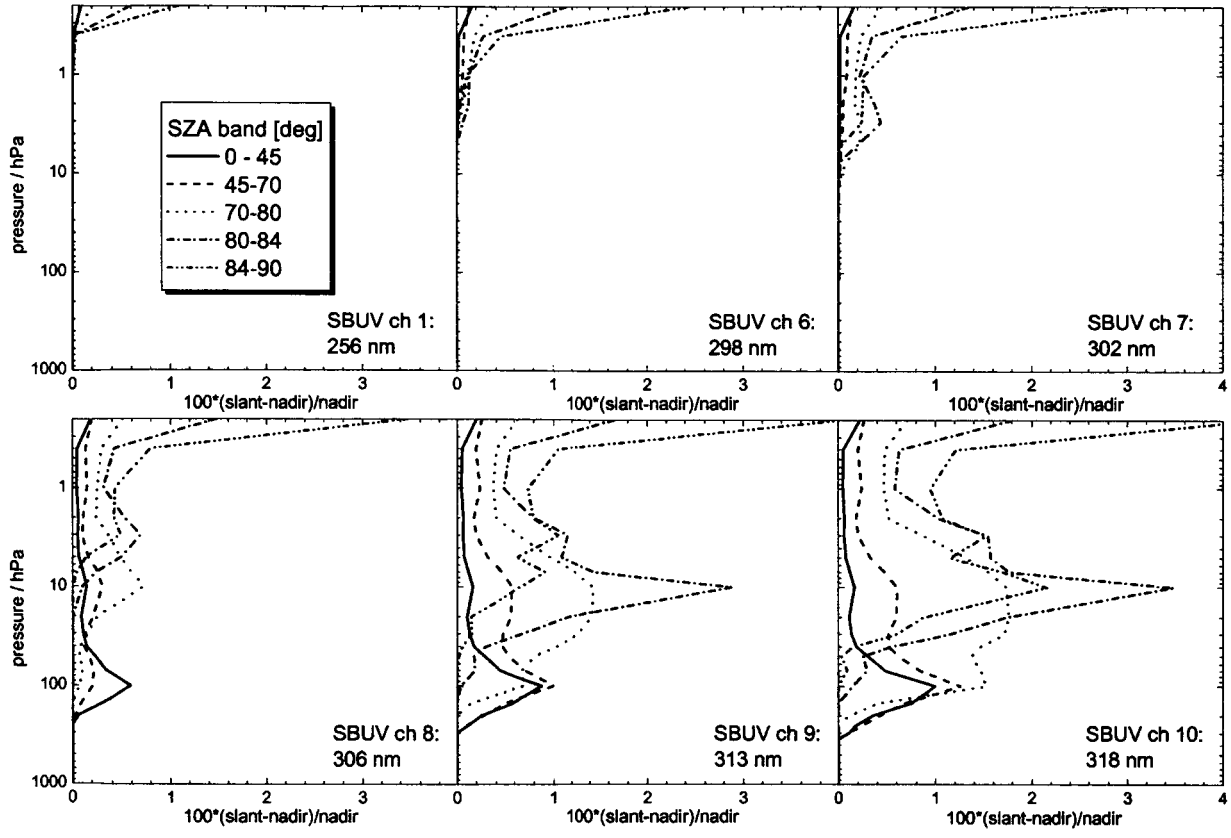

Figure 7. Standard deviation of differences between the ozone profile seen by the incoming (slant) and outgoing (nadir) radiation for SBUV channels 1 and 6 to 10.

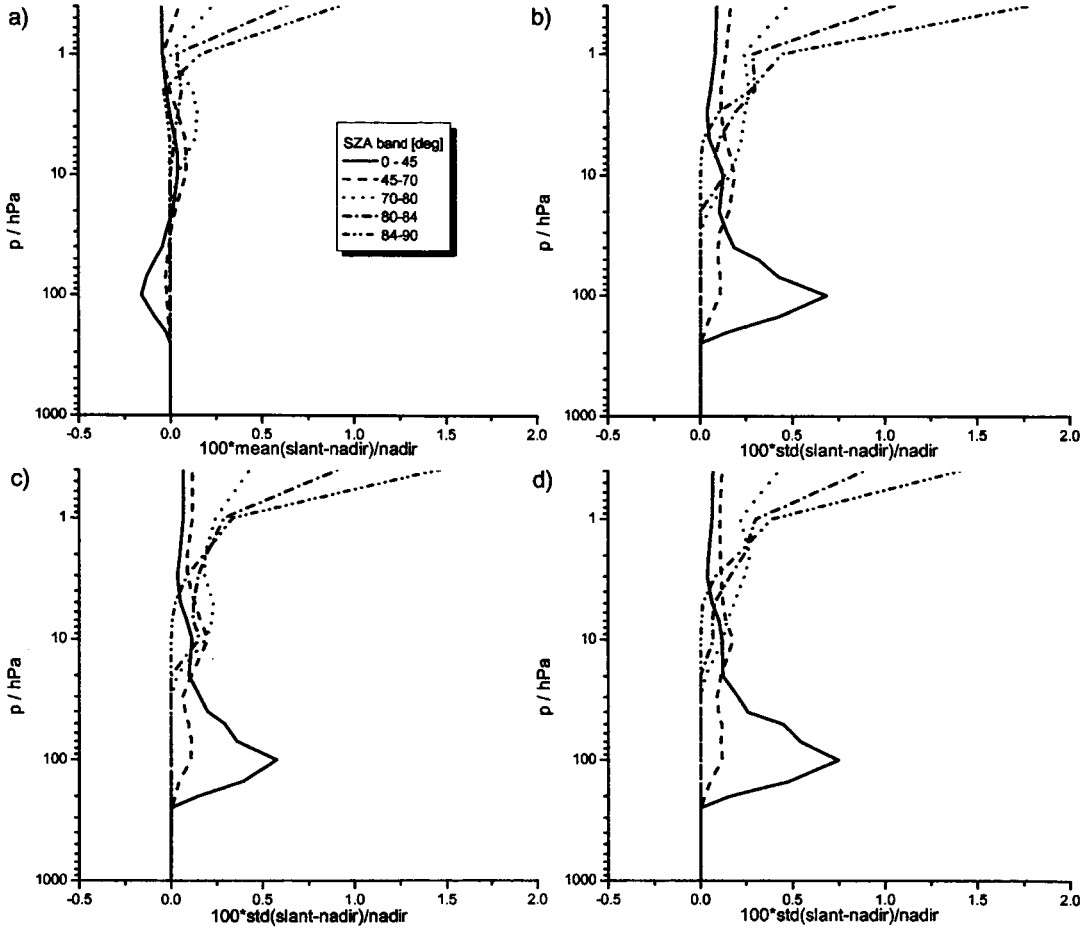

Figure 8. Same as Figure 7, but channel 8 (306 nm) only: a) mean difference. b)-d) shows similar plots for the period 2–4 March 2003, where three different atmospheric model fields were available: standard deviation (std) for b) radiance assimilation, as in Figure 7, c) profile assimilation, d) no assimilation, CTM only.

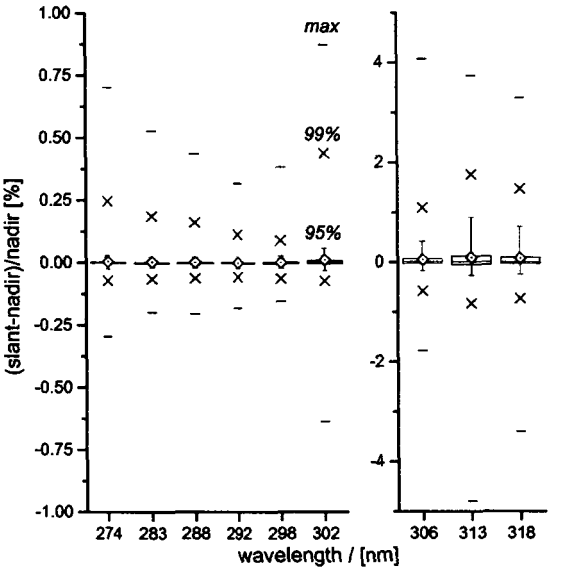

Figure 9. Box-and-whisker plots for the radiance differences of SBUV channels 2–10, on 16–17 October 2003. Boxes show the 75-percentiles and the median, the diamond marks the mean.

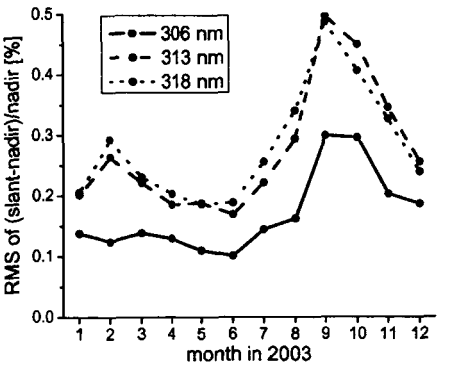

Figure 10. Variation of radiance differences over the year 2003. For each month, days 25–27 were sampled.

channel	λ actual [nm]	λ nominal [nm]	λ rounded [nm]
1	252.00	252.2	252
2	273.61	273.5	274
3	283.10	283.0	283
4	287.70	287.6	288
5	292.29	292.2	292
6	297.59	297.6	298
7	301.97	301.9	302
8	305.87	305.8	306
9	312.57	312.5	313
10	317.56	317.6	318
11	331.26	331.2	331

Table 1. SBUV/2 channels and wavelengths λ used throughout this paper. To avoid confusion, all references are made to the rounded wavelengths.

The impact of ozone field horizontal inhomogeneities on nadir-viewing orbital backscatter UV measurements

Ozone remote sounding instruments, such as the Solar Backscatter Ultra-Violet/2 (SBUV) flying on polar operational environmental satellites, provide information about vertical structure ozone that is used to determine trends including the effects of the Antarctic ozone hole. Direct measurements of the radiance that is backscattered by nitrogen, oxygen, and clouds in the atmosphere and retrievals of ozone profiles are also used in data assimilation systems for UV prediction and to improve numerical weather forecasts. The path of solar photons as they travel through the atmosphere and get scattered back to the satellite can be slanted with respect to the direction of the satellite as seen from the ground. When the expected radiance is computed using radiative transfer codes, the input atmospheric profile is assumed to be the vertical profile directly above the center of the satellite ground footprint. If horizontal variations are present in the atmospheric ozone field, the use of a vertical atmospheric profile may produce an error.

This paper attempts to quantify the effects of horizontal variations of ozone on SBUV/2 and similar instruments by computing radiances with accurate slanted atmospheric profiles and comparing them with that computed using the vertical profile above. We use slanted ozone fields from atmospheric models that include ozone and data assimilation systems that assimilate ozone information. We show that the effects of horizontal gradients on these sounders are generally small and below instrument noise. However, there are cases where the effects are greater than the instrument noise and may produce erroneous retrievals. This may happen more frequently when the most interesting atmospheric phenomena occur, such as the ozone hole and folding of the atmosphere, because these events can produce large horizontal variations in ozone. Also, due to the satellite and ozone geometry, biases may be introduced into the retrievals that in turn may produce a bias in the trends that are determined from them.

Martin Mueller, Paul Poli, Joanna Joiner

--